Article

Not peer-reviewed version

The tunable electronic and optical properties of two-dimensional bismuth oxyhalides

Yong Zhou , Beitong Cheng , Shuai Huang , Xingyong Huang , Ruomei Jiang , Xule Wang , Wei Zhang , Baonan Jia , Pengfei Lu * , Hai-Zhi Song *

Posted Date: 14 September 2023

doi: 10.20944/preprints202309.0969.v1

Keywords: 2D BiOX materials; density function theory; electronic properties; optical properties

Article

The Tunable Electronic and Optical Properties of Two-Dimensional Bismuth Oxyhalides

Yong Zhou [1,2], Beitong Cheng [1], Shuai Huang [1], Xingyong Huang [3], Ruomei Jiang [1], Xule Wang [1], Wei Zhang [1], Baonan Jia [4], Pengfei Lu [4,*] and Hai-Zhi Song [1,5,6,*]

[1] Quantum Research Center, Southwest Institute of Technical Physics, Chengdu 610041, China
[2] School of Electronic Engineering, Chengdu Technological University, Chengdu 611730, China
[3] Faculty of Science, Yibin University, Yibin 644007, China
[4] State Key Laboratory of Information Photonics and Optical Communications, Beijing University of Posts and Telecommunications, Beijing 100876, China
[5] Institute of Fundamental and Frontier Sciences, University of Electronic Science and Technology of China, Chengdu 610054, China
[6] State Key Laboratory of High Power Semiconductor Lasers, Changchun University of Science and Technology, Changchun 130013, China
* Correspondence: lupengfei@bupt.edu.cn (P.L); hzsong@uestc.edu.cn (H.Z.S); Tel.: +86-158-2823-9155 (H.Z.S)

Abstract: Two-dimensional (2D) bismuth oxyhalides (BiOX) have attracted much attention as potential optoelectronic materials. Expecting for their application diversity, we herewith systematically investigate the tunable properties of 2D BiOX by using first principles calculations. Their electronic and optical properties can be modulated by changing the number of monolayers, applying strain, and/or varying the halogen composition. The bandgap shrinks monotonically and approaches the bulk value, the optical absorption coefficient increases, and the absorption spectrum redshifts, as the layer number of 2D BiOX increases. Carrier transport property can be improved by applying tensile strain, and the ability of photocatalytic hydrogen evolution can be obtained by applying compressive strain. General strain engineering will be effective in linearly tune the bandgap of BiOX in a wide strain range. Strain together with halogen composition variation can tune the optical absorption spectrum to be on demand in the range from visible to ultraviolet. It suggests that that 2D BiOX materials have potential serving as tunable novel photodetectors, can be used to improve clean energy techniques, and are prospective in the field of flexible optoelectronics.

Keywords: 2D BiOX materials; density function theory; electronic properties; optical properties

1. Introduction

In recent years, research on two-dimensional (2D) materials has attracted significant attention [1-6]. These materials, mostly binary compounds such as transition-metal dichalcogenides [4], metal halides [5], III-V semiconductors [6] etc., often exhibit a variety of novel physical properties that are distinct from their bulk-phase counterparts [7], holding immense potential for future nano-electronic and optoelectronic applications [8-13]. Compared with 2D binary materials, ternary layered compounds possess more versatility for physical and chemical properties. Thus recently, one kind of ternary 2D compounds, bismuth oxyhalides (BiOX), have drawn increasing attentions and have emerged as a noteworthy contender with novel electronic and optical properties [14-17]. BiOX related material preparation and device fabrication have also been widely explored. In ref. [18-20], 2D BiOX (X = Cl, Br, I), layered materials have been successfully synthesized using chemical vapor deposition method and microwave technology, yielding high-performance ultraviolet photodetectors, solar cells and potential photocatalysts. However, so far found some drawbacks of BiOX, such as the relatively large bandgaps, the weak light absorption in the visible light region, the difficulty in matching water-splitting reaction etc., have limited their further application. Effective methods are strongly required to extend the application space of 2D BiOX.

2D materials often exhibit tunable properties for widening their utility [21], so the tunability of 2D BiOX is a question worth investigating. Approaches such as heterojunction formation, interface modification, enhancement of Bi content, creation of oxygen vacancies, metal/non-metal doping, layer numbers controlling, and strain engineering have provided insights for enhancing the capability of 2D BiOX [22-27]. Kong et al. have investigated the electronic structure and optical properties of single-layer BiOI under biaxial strain [28]. These few studies either applied economic simulation methods or carried out under limited conditions, giving still rather insufficient solution to optimize the property of BiOX. On the other hand, compared with 2D binary compounds, more versatile and effective tunability could be reasonably expected. It is thus our motivation to widely and systematically modulate the electronic and optical properties of 2D BiOX.

In this work, we theoretically study the behavior of BiOX by changing the layer thickness, tuning the halogen composition, and engineering the strain. The electronic and optical properties are found tunable by changing the number of layers or tuning the proportion of different halogen atoms within BiOX. Strain engineering is an effective way to tune the bandgap, band edge, and carrier transport property. It thus sheds light on the way to improve the performance of BiOX 2D materials in the field of optoelectronics.

2. Calculation methods

In this study, all calculations are performed based on the first-principles study with density functional theory (DFT) and the projector augmented wave (PAW) method [29] in the Vienna ab initio simulation package (VASP) [30]. The exchange-correlation function is treated by the Perdew-Burke-Ernzerhof (PBE) form within the generalized gradient approximation (GGA) scheme [31]. The DFT-D3 method [32,33] is adopted to describe the weak van der Waals interaction. A vacuum space of 20 Å is set in the calculation model to avoid the interaction with the adjacent layer. The energy cutoff is set as 520 eV, and the convergence criteria of force and energy are set to be 0.01 eV/Å and 1 × 10^{-5} eV/atom, respectively. When doing structural optimization, the k-point meshes are set as 9 × 9 × 3 and 9 × 9 × 1 for bulk and layered BiOX, respectively. Since PBE functional usually underestimates the band gap [28], the calculations are corrected by the more accurate hybrid function (Heyd-Scuseria-Ernzerhof (HSE06)) [34]. For strain engineering, both uniaxial and biaxial strain are set from -8% (compression) to 8% (tension) with an increment of 2%. The negative (positive) values represent compressive (tensile) strains.

The cleavage energy E_{cl} of BiOX (X = Cl, Br, I) are calculated by [35],

$$E_{cl} = \frac{E_2 - E_1}{S} \quad (1)$$

where E_1 and E_2 present the energy of system before and after exfoliation, respectively, and S is the cleavage area of the BiOX monolayer. This energy is the minimum one required to overcome the interlayer van der Waals coupling in the process of mechanical exfoliation. It can be used to evaluate the feasibility of the experimental preparation.

To estimate the stability of 2D BiOX, phonon spectra calculations are performed on a 5 × 5 × 1 supercell to evaluate their dynamic stability [36,37], and ab initio molecular dynamics (AIMD) simulations on a 4 × 4 × 1 are carried out at constant temperature (300 K) to investigate the thermodynamic stability [21,35]. Meanwhile, the cohesive energy E_c is calculated to determine the stability of BiOX by [38],

$$E_c = (\sum_i n_i E_i - E_{total})/\sum_i n_i \quad (2)$$

where i means the type of atoms, n_i is the number of type i atoms per unit cell, E_{total} represents the total energy per unit cell, and E_i is the energy of a type i atom.

The effective mass in the wave vector k direction is described by [39],

$$m^* = \frac{\hbar^2}{\partial^2 E/\partial k^2} \quad (3)$$

where $\hbar$ is the reduced Planck constant, and E is the total energy.

Preprints (www.preprints.org) | NOT PEER-REVIEWED | Posted: 14 September 2023 doi:10.20944/preprints202309.0969.v1

The optical properties are measured by the frequency (ω) dependent complex dielectric function $\varepsilon_{2D}(\omega) = \varepsilon_{1(2D)}(\omega) + i\varepsilon_{2(2D)}(\omega)$, and the refractive spectrum $n_{2D}(\omega)$ and the optical absorption spectrum $\alpha_{2D}(\omega)$ can be derived from the real part (ε_1) and the imaginary part (ε_2) [21,35,37]:

$$n_{2D}(\omega) = \left[\frac{\sqrt{\varepsilon_{1(2D)}(\omega)^2 + \varepsilon_{2(2D)}(\omega)^2} + \varepsilon_{1(2D)}(\omega)}{2}\right]^{\frac{1}{2}} \quad (4)$$

$$\alpha_{2D}(\omega) = \frac{\sqrt{2}\omega}{c}\left[\sqrt{\varepsilon_{1(2D)}(\omega)^2 + \varepsilon_{2(2D)}(\omega)^2} - \varepsilon_{1(2D)}(\omega)\right]^{\frac{1}{2}} \quad (5)$$

where c is the speed of light in vacuum.

3. Results and discussions

3.1. Crystal structure and stability

The BiOX has a unique layered structure [40] in which the $[Bi_2O_2]^{2+}$ layer is interleaved by double layers of halogen ions $[X]^-$. In the monolayer [X-Bi-O-Bi-X], each Bi atom is coordinated by four oxygen atoms and four halogen atoms, as shown in Figure 1 (a) and (b). The optimized lattice constants are calculated to be $a = b = 3.907$ Å and $c = 7.492$ Å for bulk BiOCl, $a = b = 3.943$ Å and $c = 8.258$ Å for bulk BiOBr, and $a = b = 4.02$ Å and $c = 9.271$ Å for bulk BiOI, which are in good agreement with the previous studies in both experiment and theory [20,22,41]. The calculated lattice constants of BiOX monolayer (3.876, 3.926, and 4.015 Å for BiOCl, BiOBr, and BiOI monolayer, respectively) are also consistent with previous theoretical results [27,41], verifying the validity in the optimization calculations. We have found that the optimized lattice constants (*a*) increase slightly with the number of layers, as shown in Table 1. Meanwhile, we design a new structure of bi-halogen BiOX ($X = Cl_{0.5}Br_{0.5}$, $Cl_{0.5}I_{0.5}$, $Br_{0.5}I_{0.5}$) monolayer as shown in Figure 1 (c) - (h), replacing one $[X]^-$ layer of BiOX (X = Cl, Br, I) with another halogen atoms and maintaining the tetragonal structure. The lattice constants of the BiOX (X = Cl, $Cl_{0.5}Br_{0.5}$, Br, $Cl_{0.5}I_{0.5}$, $Br_{0.5}I_{0.5}$, I) monolayer upon full relaxation by PBE-based DFT calculation are listed in Table S1, which increase monotonically with the increase of halogen atomic number.

Table 1. The calculated lattice parameters constants *a* (Å) of multi-layer BiOX (X = Cl, Br, I).

System	BiOCl	BiOBr	BiOI
		***a* (Å)**	
1 Layer	3.876	3.926	4.015
2 Layers	3.891	3.934	4.016
3 Layers	3.896	3.937	4.017
4 Layers	3.899	3.939	4.018
5 Layers	3.900	3.940	4.018
Bulk	3.907	3.943	4.020

Preprints (www.preprints.org) | NOT PEER-REVIEWED | Posted: 14 September 2023 doi:10.20944/preprints202309.0969.v1

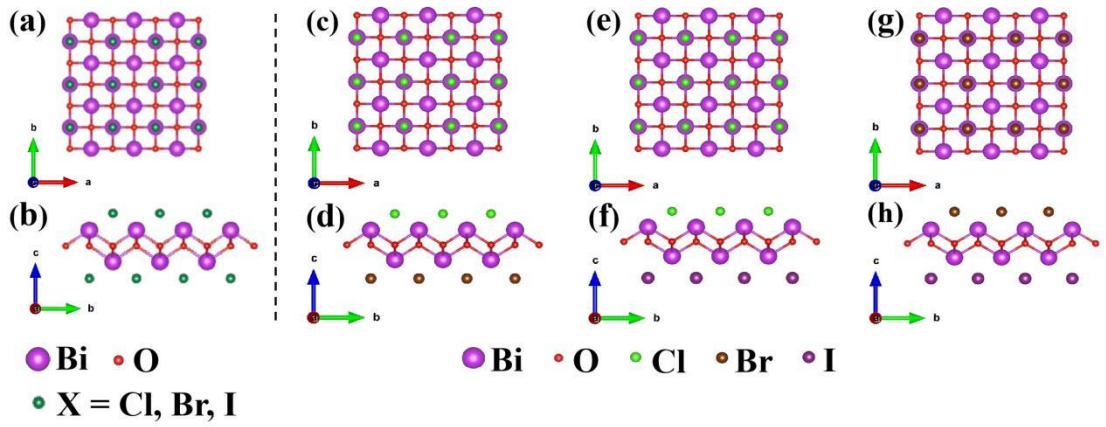

Figure 1. The top view and side view of BiOX monolayer **(a) (b)** BiOX (X = Cl, Br, I), **(c) (d)** $BiOCl_{0.5}Br_{0.5}$, **(e) (f)** $BiOCl_{0.5}I_{0.5}$, **(g) (h)** $BiOBr_{0.5}I_{0.5}$.

BiOX possesses a layered crystal structure to offer flexibility and the possibility of exfoliation into ultrathin flakes. This flexibility enables the integration of single-layer BiOX into various optoelectronic device architectures. We first try stressing the cleavage energy E_{cl} to access the feasibility of the mechanical exfoliation, as is shown in Figure 2 as a function of the distance for a BiOX (X = Cl, Br, I) monolayer to be separated from a 5-layered structure. The calculated cleavage energy of monolayer BiOCl, BiOBr and BiOI is 0.455, 0.346 and 0.302 J/m^2, respectively. Referring to those of graphene (0.37 J/m^2), single-layer SnP_3 (0.71 J/m^2) and δ-InP_3 monolayer (0.827 J/m^2) [42-44], BiOX monolayer is a fairly typical 2D material with moderate van der Waals interactions, implying that they can be easily prepared by mechanical exfoliation.

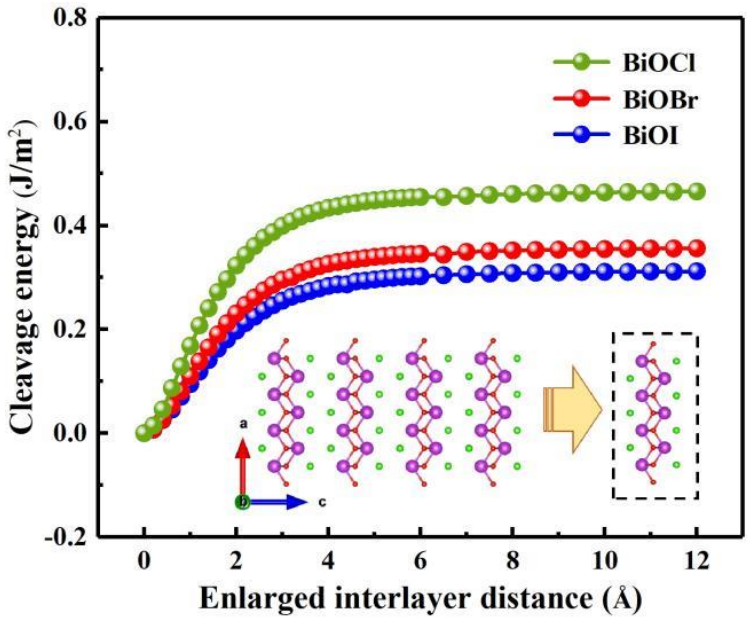

Figure 2. The cleavage energy E_{cl} (in units of J/m^2) as a function of the separation distance for five stable BiOX (X = Cl, Br, I) monolayers. Inset: isolating a monolayer from its neighboring four layers.

There is no imaginary vibration frequency observed in the phonon spectra of the BiOX monolayer, as shown in Figure S1, indicating the dynamic stability of BiOX. Meanwhile, no structure disruption occurs after 3000 fs AIMD simulations at 300 K (Figure S2), demonstrating that BiOX monolayer are thermodynamically stable. In addition, the cohesive energy was calculated to be 4.92, 4.77, 4.58, 4.84, 4.74, and 4.67 eV/atom for BiOCl, BiOBr, BiOI, $BiOCl_{0.5}Br_{0.5}$, $BiOCl_{0.5}I_{0.5}$, and $BiOBr_{0.5}I_{0.5}$

monolayer, respectively. This implies that BiOCl is the most stable among the above materials. The cohesive energy of the BiOX is greater than that of Bi_2O_2S (3.85 eV/atom) [21], p-GeN_2 (3.96 eV/atom) [45] and Silicene (3.71 eV/atom) [46], indicating their higher stability.

3.2. Thickness-dependent behavior

Because of the Van der Waals interlayer interactions, 2D materials usually possess layer-number-dependent electronic properties [47,48]. We investigate the band structure and optical properties of few-layer (two to five layers) BiOX (X = Cl, Br, I) by HSE06 functional [33]. It is first confirmed that the BiOX (X = Cl, Br, I) monolayer exhibit indirect semiconductor band structure, where the CBM is located at the Γ point while the VBM is located between the Γ and X points in the irreducible Brillouin zone. As shown in Figure 3 (a), BiOBr is taken as a representor to display the relationship between the band structure and the thickness (layer number). With increasing layer number, BiOX band structure does not change much, i.e., the CBM always stays at the Γ point, while the VBM locates along the Γ-X direction. Specifically, the VBM of BiOI moves to and then stay at the X point from 2 single layers on. It is thus clear that BiOX maintains an indirect bandgap character as the layer number increases, which may be helpful for the material design of BiOX. In the meantime, the calculated bandgaps of BiOCl, BiOBr, and BiOI monolayers are 3.745, 3.354, and 2.278 eV, respectively (Table S2), as normally expected. With increasing layer number, the bandgaps do vary as shown in Figure 3 (b). They decrease monotonically and gradually approach those of their bulks. Those of BiOCl and BiOBr monolayers are reduced obviously with the layer number due to the weak quantum size effect [41,49], but that of BiOI shows less sensitivity to the layer number, which may be due to the relatively large charge transfer and orbital hybridization between Bi and I atoms. According to the projected density of states in Figure 3 (c), the CBM is dominated by Bi 6p states, while the VBM is mainly comprised of O 2p and X *n*p (n = 3, 4, 5 for X = Cl, Br, I, respectively) states. Thus the reduced electronegativity (Cl > Br > I) can explain the decreasing band gaps. As the halogen atom X gets heavier, the contribution of X *n*p to the density of states becomes more and more obvious, and the interatomic covalent characteristics from strong to weak are in this order: Bi-O, Bi-I, Bi-Br, and Bi-Cl. The influence of I on Bi is more obvious than that of Cl and Br, so the deviation of Bi at the CBM in BiOI is more significant than those in BiOCl and BiOBr.

The thickness-dependent optical properties of BiOX (X = Cl, Br, I) is also investigated. At the same layer number, the calculated static dielectric constant $\varepsilon(0)$ and static refractive index $n(0)$ become larger with the increase of atomic number of halogen X (Table S3), as is normally expected. Figure 4 takes the optical properties of BiOCl as an example to show that the thickness dependence is similar to those of multi-layer Bi_2O_2X (X = S, Se, Te) [21] and MoS_2 [50]. As the layer thickness increases from monolayer to bulk, $\varepsilon(0)$, $n(0)$, and the optical absorption coefficient become larger, and the peaks of the imaginary part of the dielectric function and the optical absorption spectrum shift to low-energy region (redshift).

Holding the above data showing that monolayer number is effective in tuning the bandgap, dielectric constant, light absorption spectrum of 2D BiOX, one may be more achievable to design BiOX-related optoelectronic devices in extended application ranges.

Preprints (www.preprints.org) | NOT PEER-REVIEWED | Posted: 14 September 2023 doi:10.20944/preprints202309.0969.v1

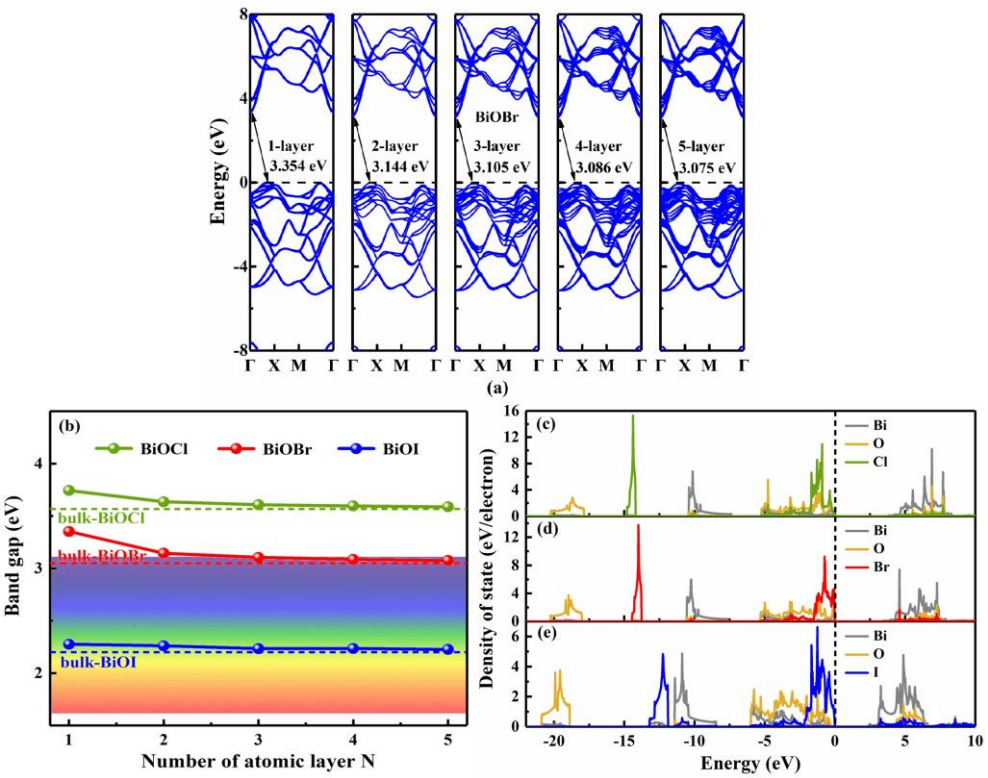

Figure 3. (a) The relationship between HSE06-based band structure of BiOBr and the layer numbers (from 1 to 5 layers), **(b)** the variation of band gap with the layer numbers of BiOX (X = Cl, Br, I), and the density of state of **(c)** BiOCl, **(d)** BiOBr, and **(e)** BiOI monolayer.

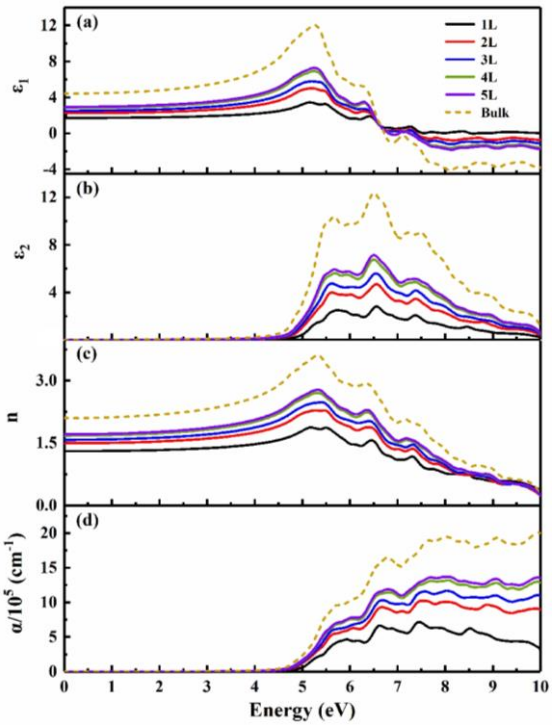

Figure 4. The optical properties of BiOCl **(a)** the real part of dielectric function ε_1, **(b)** the imaginary part of dielectric function ε_2, **(c)** the refractive index n, and **(d)** the absorption coefficient α.

3.3. Strain engineering and composition tuning

Preprints (www.preprints.org) | NOT PEER-REVIEWED | Posted: 14 September 2023 doi:10.20944/preprints202309.0969.v1

Strain engineering is often considered an effective technique for tuning the electronic structure of 2D semiconductors [21,51]. Thus we here investigate the tunable properties of 2D BiOX (X = Cl, Br, I) with strain. Figure 5 (a) depicts the band gap variation of BiOX monolayer with uniaxial and biaxial strain, and Figure S3 shows the band structures of BiOX monolayer under biaxial strain -8%, 0, and 8%. Under uniaxial strain, the band gaps of BiOCl and BiOBr monolayers decrease monotonically as the strain varies from -8% compression to 8% tension. In contrast, the band gap of BiOI decreases linearly with the increase of tensile strain, while it increases first and then decreases as the compressive strain becomes larger with a critical strain at -4%. BiOX monolayers are all indirect band gap semiconductors with or without uniaxial strain, and their CBM always remains at the Γ point. When biaxial strain is applied, the band gaps of BiOCl, BiOBr, and BiOI show similar variation trend. With the increase of compressive strain, the band gaps increase linearly first and then decrease with a critical strain at -6% and -4% for BiOCl/BiOBr and BiOI, respectively. When the compressive strain increases to -8%, the CBM of BiOX shifts from the Γ point to the M points, and in the range of compressive strain (-8%, -6%), the CBM and VBM of BiOI are located at the M point and the X point, respectively. With the increase of tensile strain, the band gaps of BiOX decrease monotonically and the CBM of BiOX remains at the Γ point. All of monotonic changes versus strain sounds almost linear, suggesting high controllability of the 2D BiOX under strain.

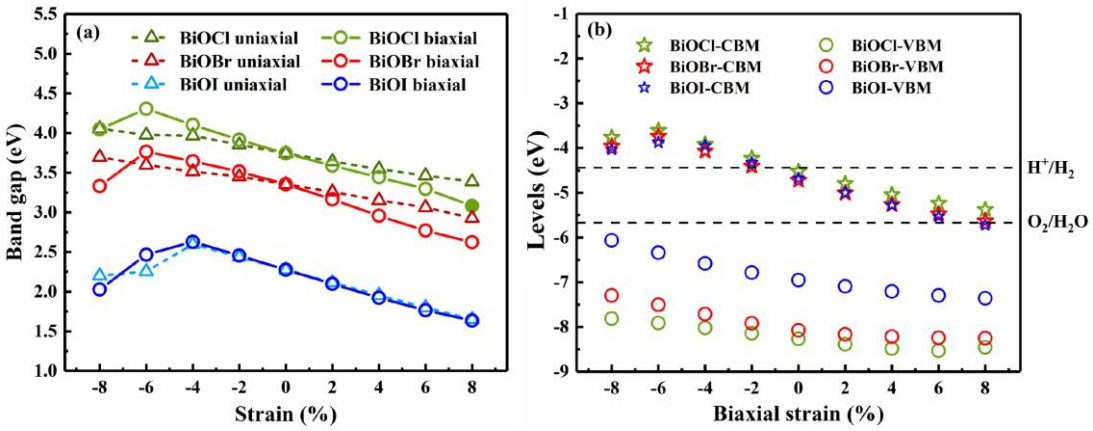

Figure 5. (a) The variation of band gap of BiOX (X = Cl, Br, I) with uniaxial and biaxial strain, and **(b)** the relationship between the band edge positions of BiOX (X = Cl, Br, I) and the biaxial strain.

In Figure S3, the CBM shows a sharper band curve, implying BiOX (X = Cl, Br, I) monolayer possesses smaller electron effective mass. Consistently, the calculated electron (hole) effective masses are 0.28 m_0 (1.33 m_0), 0.24 m_0 (1.12 m_0), and 0.19 m_0 (1.96 m_0) for BiOCl, BiOBr, and BiOI monolayer, respectively. Under tensile strain, the CBM of BiOX monolayer exhibits greater curvature than under compressive strain. It is thus expected that tensile strain will bring smaller electron effective mass and better carrier transport property than compressive strain. This is rather helpful to practical performance since tensile strain is more widely used in application of 2D materials. Under biaxial strain, both BiOBr and BiOI monolayers always exhibit indirect band gap regardless of the compressive or tensile strain applied. However, when the tensile strain increases to 8%, we have found that BiOCl monolayer has a transition from indirect band gap to direct band gap, and the CBM and VBM are both located at the Γ point. For both uniaxial and biaxial strain, the band gaps of BiOX monolayers tuned under tensile strain exhibit better linearity, while a critical strain occurs under compressive strain. The critical strain of BiOI is smaller because the smaller electronegativity of I makes it more susceptible to strain. In the strain range of (-4%, 8%), uniaxial and biaxial strain have similar influence on BiOI. BiOCl and BiOBr exhibit better tunability under biaxial strain in the strain range from -6% to 8%. Generally, the bandgap of BiOX is found tunable in a wide strain range, suggesting application potential in the fields such as flexible optoelectronics.

Preprints (www.preprints.org) | NOT PEER-REVIEWED | Posted: 14 September 2023 doi:10.20944/preprints202309.0969.v1

Band edge position is an important factor in applications such as photocatalytic water splitting [35,52,53]. As depicted in Figure 5 (b), the band edge positions of BiOX (X = Cl, Br, I) monolayer (referred to the vacuum level) shift downwards under tensile strain, and the downward trend tends to be gentler when the tensile strain goes larger. With the increase of compressive strain, the VBM position goes upwards while the CBM position shifts first upwards and then downwards with a critical strain at -6%. It is thus a feasible method to adjust the band edge positions by adopting appropriate strain. In the range of -2% to -8%, the CBM and VBM positions of strained BiOX shift upwards to higher energy positions with respect to the redox potential levels of water [27], meeting the band edges alignment requirements [53] for photocatalytic water splitting at pH = 0, that is, the CBM is higher than the reduction potential of H^+/H_2 (-4.44 eV) and the VBM is lower than the oxidation potential of O_2/H_2O (-5.67 eV). Obviously, the strain engineering has the potential to improve the photocatalytic performance of BiOX at different pH conditions. For instance, water splitting can be switched on/off simply by applying/relaxing a compressive strain, and the efficiency of photocatalytic water splitting at pH = 0 might be controlled by applying compressive strain from -2% to -8%.

The tunability of 2D BiOX is further studied by adjusting the halogen composition x in $BiOCl_xBr_{1-x}$, $BiOCl_xI_{1-x}$, and $BiOBr_xI_{1-x}$. Similar to the case x = 0.5 as in Figure 1, the models for x = 0.75, 0.875 are constructed by replacing one of the 4, 8 halogen atoms with another element in a 2 × 1 × 1, 2 × 2 × 1 supercell, respectively. In unstrained cases, the band gaps decrease gradually as the x goes smaller, making these materials suitable for absorbing wider range of visible light compared with the original BiOX (X = Cl, Br, I). Combined with strain engineering, tensile strain monotonically reduces the band gap of composition-tuned BiOX monolayer, as shown in Figure 6 (a) - (c). When the proportion of I in X is relatively large, the bandgap of BiOX is more affected by I, which may be because I is heavier and its bonding with Bi is different from Cl and Br. According to the projected density of states of $BiOBr_{0.5}I_{0.5}$ (Figure 6 (d) - (f)), the unstrained CBM is dominated by Bi 6p orbitals, while its VBM is mainly contributed by I 5p states with small amount of O 2p states. We find that there is no Br 4p states below the Fermi level, which might be due to the lower energy of Br 4p orbital than that of I 5p. With the increase of compressive strain, the contributions of I 5p states to VBM and Bi 6p states to CBM are more prominent. On the contrary, as the tensile strain increases, the contribution of O 2p and Br 4p states to VBM becomes more and more obvious. Therefore, the band gap difference between $BiOBr_{0.5}I_{0.5}$ and BiOI becomes greater with the increase of the tensile strain. These results indicate that both composition tuning and strain engineering are effective ways to tune the band gap of BiOX (X = Cl, Br, I). It is predicted that composition tuning and/or tensile strain can decrease the band gap, enhance the optical absorption coefficients and the photocatalyst activity of BiOCl and BiOBr in the visible light region. This flexibility in bandgap tuning will benefit the material design of 2D BiOX and its applications in optoelectronic devices. As a whole, although those with I is weakly changeable when $x \leq 0.5$, these BiOX exhibit effective controllability under composition tuning, which is beneficial to many applications.

Preprints (www.preprints.org) | NOT PEER-REVIEWED | Posted: 14 September 2023 doi:10.20944/preprints202309.0969.v1

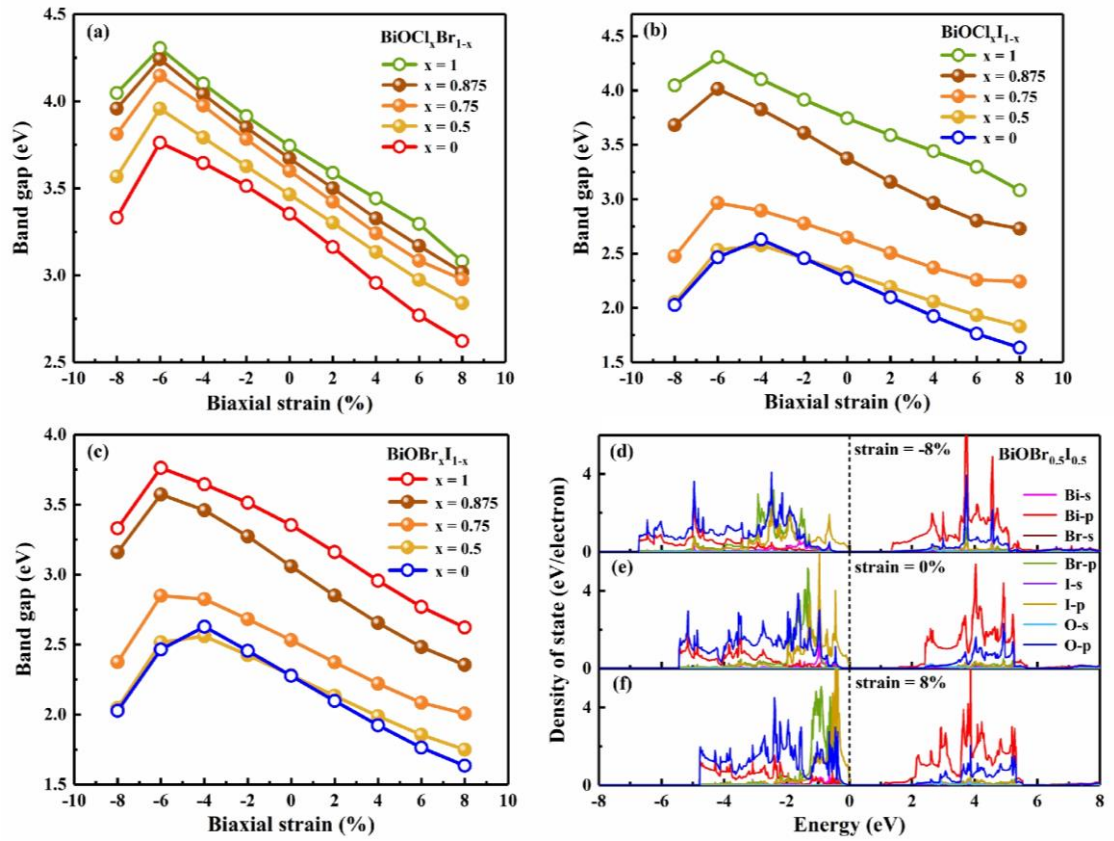

Figure 6. The variation of band gap with the halogen proportion x (x = 1, 0.875, 0.75, 0.5, 0) and the biaxial strain for **(a)** BiOCl$_x$Br$_{1-x}$, **(b)** BiOCl$_x$I$_{1-x}$, **(c)** BiOBr$_x$I$_{1-x}$, and the density of state of BiOBr$_{0.5}$I$_{0.5}$ under biaxial strain **(d)** -8%, **(e)** 0%, **(f)** 8%.

Next we try studying the optical properties, as are important to optoelectronic materials [18,52], of BiOX (X = Cl, Br, I, Cl$_{0.5}$Br$_{0.5}$, Cl$_{0.5}$I$_{0.5}$, Br$_{0.5}$I$_{0.5}$). For unstrained BiOX, the static dielectric constant $\varepsilon(0)$ and the static refractive index $n(0)$ decrease in the order of BiOI, BiOBr$_{0.5}$I$_{0.5}$, BiOCl$_{0.5}$I$_{0.5}$, BiOBr, BiOCl$_{0.5}$Br$_{0.5}$, and BiOCl. This order follows the decreasing average atomic number of halogen X, so it naturally brings about the blueshifting absorption spectrum as shown in Figure 7 (a). This shift suggests that the absorption spectrum can be tuned on demand in the range from visible to ultraviolet. Specifically, BiOI, BiOBr$_{0.5}$I$_{0.5}$ and BiOCl$_{0.5}$I$_{0.5}$ maintain absorption coefficient as high as 10^4 - 10^5 cm^{-1} within the energy range of ~ 3.1 - 4.1 eV. These materials may thus be used to compensate the absorption drawback of silicon solar cells in this range to improve the utilization rate of solar energy. Hence the halogen composition tuning enhances the application potential of BiOX in the visible to violet region. With applied strains, the $\varepsilon(0)$ and $n(0)$ change slightly, suggesting a certain stability as the material is tuned by strain. As represented by BiOBr, Figure 7 (b) shows the absorption spectra under strains. It is observed that the optical absorption edges and the absorption peaks redshift under tensile strain, which can improve the ability of absorbing visible light. As the compressive strain increases from 0% to -6%, the optical absorption edges blueshift. Together with the fact that the absorption coefficients of strained BiOX in the ultraviolet region is not degraded by compressive or tensile strain, the above properties imply that BiOX has application potential in flexible optoelectronic devices.

Preprints (www.preprints.org) | NOT PEER-REVIEWED | Posted: 14 September 2023 doi:10.20944/preprints202309.0969.v1

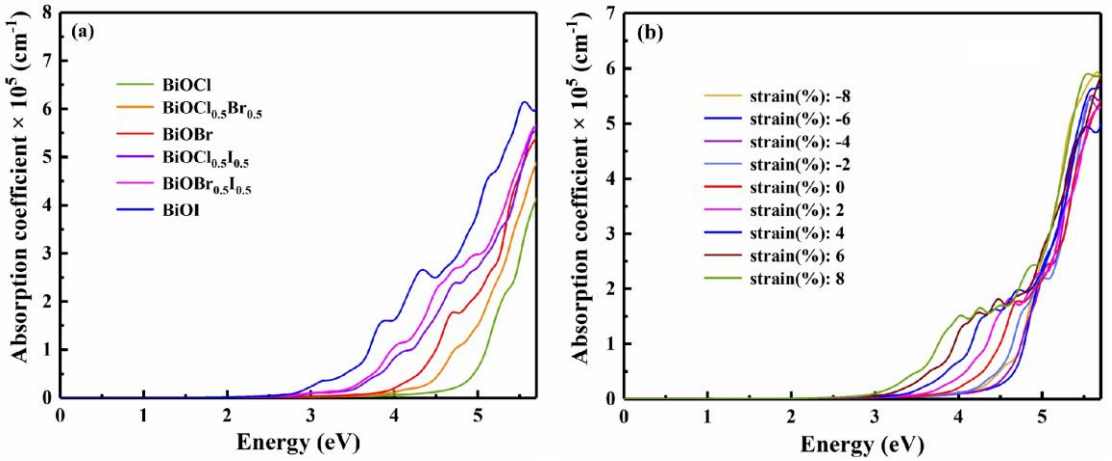

Figure 7. (a) The optical absorption spectra of the BiOX (X = Cl, $Cl_{0.5}Br_{0.5}$, Br, $Cl_{0.5}I_{0.5}$, $Br_{0.5}I_{0.5}$, I) monolayer, and **(b)** the variation of the optical absorption spectrum of BiOBr with biaxial strain.

4. Conclusions

In this study, we systematically investigate the properties of 2D BiOX materials. The electronic and optical behaviors of 2D BiOX can be tuned by changing the layer number, varying the halogen composition, and/or applying strain. As the layer number of 2D BiOX increases, the bandgap decreases monotonically and gradually approaches that of the bulk material, the optical absorption coefficient increases, and the absorption spectrum redshifts. Tensile strain can be expected to bring better carrier transport property, and compressive strain can switch BiOX into material capable of photocatalyst water-splitting. More generally, strain engineering in a wide range can linearly modulate the bandgap of BiOX. Strain application and/or halogen composition variation will be effective to tune the optical absorption spectrum being on demand in the range from visible to ultraviolet. The observed tunability of 2D BiOX can be expected to extend their application range, to optimize photodetection performance, to improve clean energy technology, and to realize novel flexible optoelectronic devices.

Author Contributions: Y.Z.: Model building, simulation, data processing, and writing-original draft; Y.Z., X.H., B.C., R.J., X.W., W.Z and B.J.: Investigation help and discussion; H.S.: Writing and revising guidance, project administration, resources, supervision. All authors have read and agreed to the published version of the manuscript.

Funding: This research was supported by the National Key Research and Development Program of China under grants 2019YFB2203400 and 2021YFA0718803, and by the National Science Foundation of Sichuan Province under grant 2022NSFSC1817. We also acknowledge the support of the Special Subject of Significant Science and Technology of Sichuan Province under grant 2018TZDZX0001 and the Special Subject of Significant Innovation of Chengdu City under grant 2021-YF08-00159-GX.

Data Availability Statement: The data presented in this study are available on request from the corresponding author.

Conflicts of Interest: The authors declare no conflict of interest.

References

1. Novoselov, K. S.; Geim, A. K.; Morozov, S. V.; Jiang, D.; Zhang, Y.; Dubonos, S. V.; Grigorieva, I. V.; Firsov, A. A. Electric field effect in atomically thin carbon films. *Science* **2004**, *306(5659)*, 666-669.
2. Liu, H.; Neal, A. T.; Zhu, Z.; Luo, Z.; Xu, X.; Tománek, D.; Ye, P. D. Phosphorene: an unexplored 2D semiconductor with a high hole mobility. *ACS nano* **2014**, *8(4)*, 4033-4041.
3. Mannix, A. J.; Zhou, X. F.; Kiraly, B.; Wood, J. D.; Alducin, D.; Myers, B. D.; Liu, X.; Fisher, B. L.; Santiago, U.; Guest, J. R.; Yacaman, M. J.; Ponce, A.; Oganov, A. R.; Hersam, M. C.; Guisinger, N.P. Synthesis of borophenes: Anisotropic, two-dimensional boron polymorphs. *Science* **2015**, *350(6267)*, 1513-1516.
4. Jacoby, M. 2-D materials go beyond graphene. *Chemical & Engineering News* **2017**, *95(22)*, 36.

5. Huang, X.; Zhuo, Z.; Yan, L.; Wang, Y.; Xu, N.; Song, H. Z.; Zhou, L. Single-Layer Zirconium Dihalides ZrX_2 (X = Cl, Br, and I) with Abnormal Ferroelastic Behavior and Strong Anisotropic Light Absorption Ability. *The journal of physical chemistry letters* **2021**, *12(32)*, 7726-7732.
6. Sahin, H.; Cahangirov, S.; Topsakal, M.; Bekaroglu, E.; Akturk, E.; Senger, R. T.; Ciraci, S. Monolayer honeycomb structures of group-IV elements and III-V binary compounds: First-principles calculations. *Physical Review B* **2009**, *80(15)*, 155453.
7. Butler, S. Z.; Hollen, S. M.; Cao, L.; Cui, Y.; Gupta, J. A.; Gutiérrez, H. R.; Heinz, T. F.; Hong, S. S.; Huang, J.; Ismach, A. F.; Johnston-Halperin, E.; Kuno, M.; Plashnitsa, V. V.; Robinson, R. D.; Ruoff, R. S.; Salahuddin, S.; Shan, J.; Shi, L.; Spencer, M. G.; Terrones, M.; Windl, W.; Goldberger, J. E. Progress, challenges, and opportunities in two-dimensional materials beyond graphene. *ACS nano* **2013**, *7(4)*, 2898-2926.
8. Bao, Q.; Loh, K. P. Graphene photonics, plasmonics, and broadband optoelectronic devices. *ACS nano* **2012**, *6(5)*, 3677-3694.
9. Koppens, F. H.; Mueller, T.; Avouris, P.; Ferrari, A. C.; Vitiello, M. S.; Polini, M. Photodetectors based on graphene, other two-dimensional materials and hybrid systems. *Nat Nanotechnol* **2014**, *9(10)*, 780-793.
10. Li, D.; Gong, Y.; Chen, Y.; Lin, J.; Khan, Q.; Zhang, Y.; Li, Y.; Zhang, H.; Xie, H. Recent Progress of Two-Dimensional Thermoelectric Materials. *Nano-micro letters* **2020**, *12(1)*, 535-549.
11. Li, F.; Shen, T.; Wang, C.; Zhang, Y.; Qi, J.; Zhang, H. Recent Advances in Strain-Induced Piezoelectric and Piezoresistive Effect-Engineered 2D Semiconductors for Adaptive Electronics and Optoelectronics. *Nano-micro letters* **2020**, *12(1)*, 106.
12. Li, X.; Yang, J. First-principles design of spintronics materials. *National Science Review* **2016**, *3(3)*, 365-381.
13. Lightcap, I.; T. Kosel, P.V. Kamat, Anchoring semiconductor and metal nanoparticles on a two-dimensional catalyst mat. Storing and shuttling electrons with reduced graphene oxide. *Nano Letters* ***2010***, *10(2)*, 577-583.
14. Wu, S.; Wu, D. First principle calculations of photocatalytic properties of bismuth oxyhalides considering van der Waals correction. *2016 IEEE International Conference on Electro Information Technology (EIT)*, Grand Forks, ND, USA **2016**, 0452-0457.
15. Ye, L.; Wang, L.; Xie, H.; Su, Y.; Jin, X.; Zhang, C. Two-Dimensional Layered BiOX (X=Cl, Br) Compounds as Anode Materials for Lithium-Ion Batteries. *Energy Technol* **2015**, *3(11)*, 1115-1120.
16. Xu, K.; Wang, L.; Xu, X.; Dou, S. X.; Hao, W.; Du, Y. Two-dimensional bismuth-based layered materials for energy-related applications. *Energy Storage Materials* **2019**, *19*, 446-463.
17. Di, J.; Xia, J.; Li, H.; Guo, S.; Dai, S. Bismuth oxyhalide layered materials for energy and environmental applications. *Nano Energy* **2017**, *41*, 172-192.
18. Kang, L.; Yu, X.; Zhao, X.; Ouyang, Q.; Di, J.; Xu, M.; Tian, D.; Gan, W.; Ang, C. C. I.; Ning, S.; Fu, Q.; Zhou, J.; Kutty, R. G.; Deng, Y.; Song, P.; Zeng, Q.; Pennycook, S. J.; Shen, J.; Yong, K. T.; Liu, Z. Space-confined microwave synthesis of ternary-layered BiOCl crystals with high-performance ultraviolet photodetection. *InfoMat* **2020** *2(3)*, 593-600.
19. Zeng, W.; Li, J.; Feng, L.; Pan, H.; Zhang, X.; Sun, H.; Liu, Z. Synthesis of large-area atomically thin BiOI crystals with highly sensitive and controllable photodetection. *Advanced Functional Materials* **2019**, *29(16)*, 1900129.
20. Liu, P.; Yin, L.; Feng, L.; Sun, Y.; Sun, H.; Xiong, W.; Xia, C.; Wang, Z.; Liu, Z. Controllable preparation of ultrathin 2D BiOBr crystals for high-performance ultraviolet photodetector. *Science China Materials* **2021**, *64(1)*, 189-197.
21. Li, J. Q.; Cheng, C.; Duan, M. Y. The electronic and optical properties of multi-layer Bi_2O_2X (X = S, Se, Te) by first-principles calculations. *Applied Surface Science* **2023** *618*, 156541.
22. Wang, G.; Luo, X.; Huang, Y.; Kuang, A.; Yuan, H.; Chen, H. BiOX/BiOY (X, Y = F, Cl, Br, I) superlattices for visible light photocatalysis applications. *RSC advances*, **2016**, *6*, 91508-91516.
23. Zhao, A.; Zhang, L.; Guo, Y.; Li, H.; Ruan, S.; Zeng, Y. J. Emerging members of two-dimensional materials: bismuth-based ternary compounds. *2D Materials* **2021** *8(1)*, 012004.
24. Bhachu, D. S.; Moniz, S. J. A.; Sathasivam, S.; Scanlon, D. O.; Walsh, A.; Bawaked, S. M.; Mokhtar, M.; Obaid, A. Y.; Parkin, I. P.; Tang, J.; Carmalt, C. J. Bismuth oxyhalides: synthesis, structure and photoelectrochemical activity. *Chem Sci.* **2016** *7(8)*, 4832-4841.
25. Ye, L.; Su, Y.; Jin, X.; Xie, H. Zhang, C. Recent advances in BiOX (X = Cl, Br and I) photocatalysts: synthesis, modification, facet effects and mechanisms. *Environmental Science: Nano* **2014** *1(2)*, 90-112.
26. Zhao, Z. Y.; Dai, W. W. Structural, Electronic, and Optical Properties of Eu-Doped BiOX (X = F, Cl, Br, I): A DFT+U Study. *Inorganic Chemistry* **2014** *53(24)*, 13001-13011.
27. Wang, J.; Zhang, M.; Meng, J.; Li, Q.; Yang, J. Single- and few-layer BiOI as promising photocatalysts for solar water splitting. *RSC Advances* **2017** *7(39)*, 24446-24452.
28. Kong, T.; Wei, X.; Zhu, G.; Huang, Y. Electronic structure and optical properties of BiOI {001} monolayer under biaxial strain. *Journal of Materials Science* **2018**, *53(1)*, 708-715.

29. Hafner, J. Ab-initio simulations of materials using VASP: Density-functional theory and beyond. *Journal of computational chemistry* **2008**, *29(13)*, 2044-2078.
30. Sun, G.; Kürti, J.; Rajczy, P.; Kertesz, M.; Hafner, J.; Kresse, G. Performance of the Vienna ab initio simulation package (VASP) in chemical applications. *Journal of Molecular Structure: THEOCHEM* **2003**, *624*(1-3), 37-45.
31. Perdew, J. P.; Burke, K.; Ernzerhof, M. Generalized Gradient Approximation Made Simple. *Physical Review Letters* **1996** *77(18)*, 3865-3868.
32. Grimme, S. Semiempirical GGA-type density functional constructed with a long-range dispersion correction. *Journal of computational chemistry* **2006**, *27(15)*, 1787-1799.
33. Kerber, T.; Sierka, M.; Sauer, J. Application of semiempirical long-range dispersion corrections to periodic systems in density functional theory. *Journal of computational chemistry* **2008**, *29(13)*, 2088-2097.
34. Heyd, J.; Scuseria, G. E.; Ernzerhof, M. Hybrid functionals based on a screened Coulomb potential. *The journal of chemical physics* **2003**, *118(18)*, 8207-8215.
35. Huang, X.; Yan, L.; Zhou, Y.; Wang, Y.; Song, H. Z.; Zhou, L. Group 11 Transition-Metal Halide Monolayers: High Promises for Photocatalysis and Quantum Cutting. *The journal of physical chemistry letters* **2021**, *12(1)*, 525-531.
36. Wang, N.; Li, M.; Xiao, H. Y.; Gao, Z.; Liu, Z. J.; Zu, X.; Li, S.; Qiao, L. Band degeneracy enhanced thermoelectric performance in layered oxyselenides by first-principles calculations. *npj Computational Materials* **2021**, *7(1)*, 18.
37. Wang, V.; Xu, N.; Liu, J. C.; Tang, G.; Geng, W. VASPKIT: A user-friendly interface facilitating high-throughput computing and analysis using VASP code. *Computer Physics Communications* **2021**, *267*, 108033.
38. Zhang, C. G.; Ji, W. X.; Li, S. S.; Li, P.; Zhang, C. W.; Wang, P. J. 2D ternary nitrides XNY (X=Ti, Zr, Hf; Y=F, Cl, Br) with applications as photoelectric and photocatalytic materials featuring mechanical and optical anisotropy: A DFT study. *Journal of Solid State Chemistry* **2021**, *303(366)*, 122517.
39. Qiao, J.; Kong, X.; Hu, Z. X.; Yang, F.; Ji, W. High-mobility transport anisotropy and linear dichroism in few-layer black phosphorus. *Nature communications* **2014**, *5*, 4475.
40. Bannister, F. A. The Crystal-Structure of the Bismuth Oxyhalides. *Mineralogical Magazine* **1935**, *24(149)*, 49-58.
41. Zhang, X.; Li, B.; Wang, J.; Yuan, Y.; Zhang, Q.; Gao, Z.; Liu, L. M.; Chen, L. The stabilities and electronic structures of single-layer bismuth oxyhalides for photocatalytic water splitting. *Physical Chemistry Chemical Physics* **2014**, *16(47)*, 25854-25861.
42. Zacharia, R.; Ulbricht, H.; Hertel, T. Interlayer cohesive energy of graphite from thermal desorption of polyaromatic hydrocarbons. *Physical Review B* **2004**, *69(15)*, 155406.
43. Ghosh, B.; Puri, S.; Agarwal, A.; Bhowmick, S. SnP_3: A Previously Unexplored Two-Dimensional Material. *The Journal of Physical Chemistry C* **2018**, *122(31)*, 18185−18191.
44. Yi, W.; Chen, X.; Wang, Z.; Ding, Y.; Yang, B.; Liu, X. A novel two-dimensional δ-InP_3 monolayer with high stability, tunable bandgap, high carrier mobility, and gas sensing of NO_2. *Journal of Materials Chemistry C* **2019**, *7(24)*, 7352-7359.
45. Liu, J.; Shen, Y.; Lv, L.; Gao, X.; Meng, X.; Zhou, M.; Yang, X.; Zhang, Y.; Zheng, Y.; Zhou, Z. Mechanical, electronic and photocatalytic properties of binary Ge-based materials GeX_2 (X = B, C, N) with a pentagonal structure. *Journal of Materials Chemistry C* **2022**, *10(27)*, 10147-10156.
46. Li, Y.; Liao, Y.; Chen, Z. Be_2C Monolayer with Quasi-Planar Hexacoordinate Carbons: A Global Minimum Structure. *Angewandte Chemie International Edition* **2014**, *53(28)*, 7248-7252.
47. Liu, C. H.; Li, Z.; Mak, K. F.; Cappelluti, E.; Heinz, T. F. Observation of an electrically tunable band gap in trilayer graphene. *Nature Physics* **2011**, *7(12)*, 944-947.
48. Dai, J.; Zeng, X. C. Bilayer Phosphorene: Effect of Stacking Order on Bandgap and Its Potential Applications in Thin-Film Solar Cells. *The journal of physical chemistry letters* **2014**, *5(7)*, 1289-1293.
49. Hu, C. W.; Yang, Y.; Hou, C.; Liang, T. X. Thickness- and strain-tunable electronic structures of two-dimensional Bi_2O_2Se. *Computational Materials Science* **2021**, *194*, 110424.
50. Kumar, A.; Ahluwalia, P. K. A first principle comparative study of electronic and optical properties of 1H-MoS_2 and 2H-MoS_2. *Materials Chemistry and Physics* **2012**, *135(2-3)*, 755-761.
51. Fei, R.; Yang, L. Strain-engineering the anisotropic electrical conductance of few-layer black phosphorus. *Nano Letters* **2014**, *14(5)*, 2884-2889.
52. Zhang, X.; Zhao, X.; Wu, D.; Jing, Y.; Zhou, Z. $MnPSe_3$ monolayer: a promising 2D visible-light photohydrolytic catalyst with high carrier mobility. *Advanced Science* **2016**, *3(10)*, 1600062.
53. Gupta, U.; Rao, C. N. R. Hydrogen generation by water splitting using MoS_2 and other transition metal dichalcogenides. *Nano Energy* **2017**, *41*, 49-65.
54. Zhang, Z.; Su, J.; Hou, J.; Lin, Z.; Hu, Z.; Chang, J.; Zhang, J.; Hao, Y. Potential applications of halide double perovskite Cs_2AgInX_6 (X = Cl, Br) in flexible optoelectronics: unusual effects of uniaxial strains. *The journal of physical chemistry letters* **2019**, *10(5)*, 1120-1125.